LETTERS
https://doi.org/10.1038/s41550-018-0667-x

nature astronomy

Corrected: Publisher Correction

A circumbinary protoplanetary disk in a polar configuration

Grant M. Kennedy[1,2*], Luca Matrà[3], Stefano Facchini[4,5], Julien Milli[6], Olja Panić[7], Daniel Price[8,9], David J. Wilner[3], Mark C. Wyatt[10] and Ben M. Yelverton[10]

Nearly all young stars are initially surrounded by 'protoplanetary' disks of gas and dust, and in the case of single stars at least 30% of these disks go on to form planets[1]. The process of protoplanetary disk formation can result in initial misalignments, where the disk orbital plane is different from the stellar equator in single-star systems, or different from the binary orbital plane in systems with two stars[2]. A quirk of the dynamics means that initially misaligned 'circumbinary' disks—those that surround two stars—are predicted to evolve to one of two possible stable configurations: one where the disk and binary orbital planes are coplanar and one where they are perpendicular (a 'polar' configuration)[3–5]. Previous work has found coplanar circumbinary disks[6], but no polar examples were known until now. Here, we report the first discovery of a protoplanetary circumbinary disk in the polar configuration, supporting the predictions that such disks should exist. The disk shows some characteristics that are similar to disks around single stars, and that are attributed to dust growth. Thus, the first stages of planet formation appear able to proceed in polar circumbinary disks.

The process of star and disk formation is not guaranteed to yield a simple coplanar circumstellar disk, as might be surmised from the coplanar nature of the Solar System. Simulations suggest that once a protoplanetary disk has initially formed around a star or stars, further accretion of material with different angular momenta can result in disks with multiple orbital planes, or disks whose orbital planes are different from the binary stars they orbit[2]. IRS 43 appears to be a very young system with a misaligned circumbinary disk[7]—evidence that the initial conditions suggested by simulations do indeed occur.

Theory suggests that circumbinary disks should then evolve to one of two possible configurations—a quirk dictated by the orbital dynamics around two stars. For small initial misalignments, the angular momentum vector of circumbinary orbits $\mathbf{L}_c$ precesses about the binary angular momentum vector $\mathbf{L}_b$ (a 'coplanar' family of orbits), but for larger misalignments $\mathbf{L}_c$ precesses about a vector in the binary's pericentre direction $\boldsymbol{\varpi}_b$ (a 'polar' family)[8]. Because the disks that orbit young stars are gas rich and hence dissipative, an initially misaligned circumbinary disk will generally evolve to an end state that belongs to one of these two families[3–5,9–11]. The expected timescale for this reorientation is generally shorter than the typical ~3 Myr disk lifetime[12], meaning that young gas-rich circumbinary disks are most likely to be observed to be in one of the two possible orientations, rather than at an intermediate orientation. While the circumbinary debris disk 99 Herculis is thought to have a polar configuration[13], this disk is four times larger than Neptune's orbit and, with an age similar to the Solar System, does not provide evidence that young gas-rich polar circumbinary disks exist.

Here, we report that the circumbinary disk in the young HD 98800 system is strongly misaligned with the binary orbital plane. We infer that the disk is in the polar configuration by simulating the disk dynamics. We further show that despite this misalignment, the disk shows physical properties similar to disks seen around young single stars.

The HD 98800 system is a well-known hierarchical quadruple star system 44.9 parsecs from Earth[14], and a member of the ~10-Myr-old TW Hydrae association[15,16]. It consists of two pairs of binaries (called 'A' and 'B', or equally 'AaAb' and 'BaBb') with semi-major axes of about 1 astronomical unit (AU), which themselves orbit each other with a semi-major axis of 54 AU. The binary BaBb is well characterized[17], with an eccentricity of 0.785 ± 0.005, an ascending node of $337.6 \pm 2.4°$ anti-clockwise from north and an inclination of $67 \pm 3°$. Using the new data presented here, we derive a new orbit for AB (see Supplementary Information), which has an eccentricity of 0.52 ± 0.01 and a period of 246 ± 5 years, with an ascending node of $4.7 \pm 0.2°$ and an inclination of $88.4 \pm 2°$. These orbits, as projected on the sky plane, are shown in Fig. 1. The AaAb orbit is less certain, but the details do not affect our conclusions.

The northern pair known as HD 98800BaBb has been known to host a bright circumbinary disk since its discovery in the 1980s[18]. The disk is thought to be influenced by the stellar system[19], with the inner edge of the disk truncated by the inner binary BaBb, and the outer edge externally truncated by A[20,21]. The orientation of the disk was initially thought to be coplanar with the inner binary[20], but higher-resolution observations suggest a different orientation[21] (see Methods for a comparison with our results). Whether the disk harbours a significant mass of gas has been unclear, meaning that it has been interpreted as both a gas-rich 'protoplanetary' disk[21,22] and a gas-poor 'debris' disk[23]. The detection of oxygen towards the system[24], and molecular hydrogen emission towards B[25], suggests that this pair is accreting from a gas-rich disk, favouring the gas-rich 'protoplanetary' disk interpretation.

To ascertain the disk orientation, size, structure and evolutionary status, we observed the HD 98800 system with the Atacama Large Millimeter/submillimeter Array (ALMA; see Methods). Data were taken at 230 GHz (1.3 mm), to image dust continuum emission and the carbon monoxide $J = 2–1$ rotational transition, and

[1]Department of Physics, University of Warwick, Coventry, UK. [2]Centre for Exoplanets and Habitability, University of Warwick, Coventry, UK. [3]Harvard-Smithsonian Center for Astrophysics, Cambridge, MA, USA. [4]Max-Planck-Institut für Extraterrestrische Physik, Garching, Germany. [5]European Southern Observatory, Garching, Germany. [6]European Southern Observatory, Santiago, Chile. [7]School of Physics and Astronomy, University of Leeds, Leeds, UK. [8]Monash Centre for Astrophysics, Monash University, Melbourne, Victoria, Australia. [9]School of Physics and Astronomy, Monash University, Melbourne, Victoria, Australia. [10]Institute of Astronomy, University of Cambridge, Cambridge, UK. *e-mail: g.kennedy@warwick.ac.uk

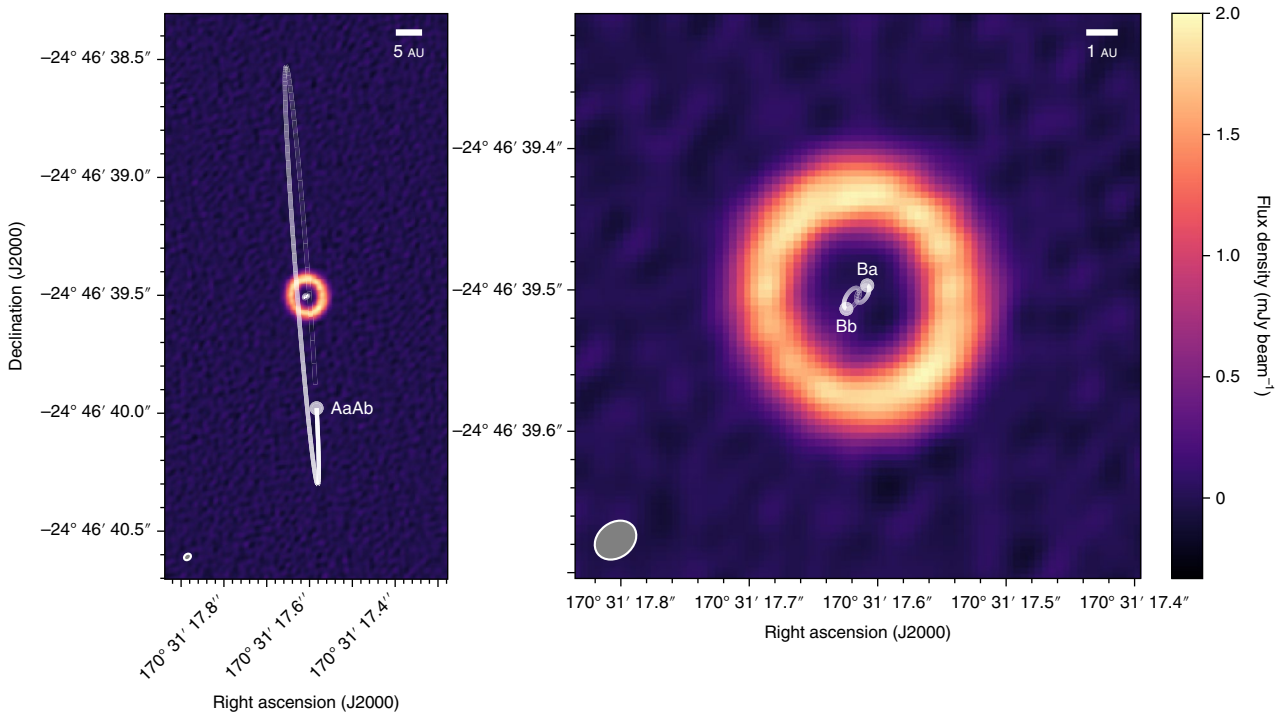

Fig. 1 | ALMA 1.3 mm continuum image of the HD 98800 dust disk, showing a narrow dust ring 3.5 AU in radius that is 2 AU wide. White semi-transparent lines show the orbits of the inner binary (BaBb) and the path of the outer binary (AaAb) with respect to BaBb, with dots at the star locations at the time of the ALMA observation. The resolution of these 'uniformly weighted' images (32 × 25 milliarcsec^2, or 1.4 × 1.1 AU^2) is given by the ellipse in the lower left corner. Left, entire system. Right, magnification of BaBb.

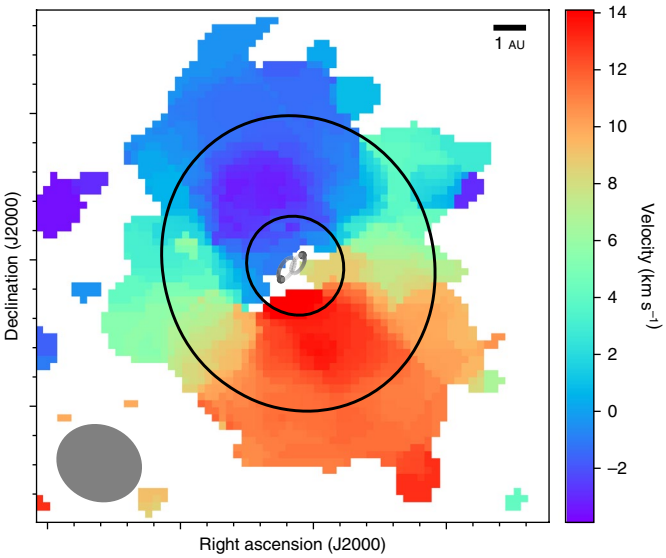

Fig. 2 | Carbon monoxide gas velocity map. Colours show the intensity-weighted carbon monoxide velocity, and contours the dust. The gas velocity structure is consistent with that expected if the carbon monoxide disk has the same orientation as the dust. The carbon monoxide is only shown where it is detected at a signal-to-noise ratio greater than 3, and the contours are shown at 20 times the noise level in the continuum image, giving an indication of the location and extent of the dust ring. The resolution of these 'naturally weighted' images (61 × 54 milliarcsec^2, or 2.7 × 2.4 AU^2) is given by the ellipse in the lower left corner. As in the right panel of Fig. 1, major axis ticks are 0.1 arcsec apart.

both are strongly detected (Figs. 1 and 2). By modelling these data as a disk that lies between inner and outer radii with a power-law surface brightness prescription, we find that the inner edges of the dust and carbon monoxide are at 2.5 ± 0.02 and 1.6 ± 0.3 AU, respectively, while the outer edges are at 4.6 ± 0.01 and 6.4 ± 0.5 AU (see Methods). These models show that the disk is largely axisymmetrical, although a small asymmetry in the dust distribution at the inner edge may be a sign of interaction with the binary. The dust and carbon monoxide components are consistent with having the same orientation; the disk has a position angle of 16 ± 1° (measured anticlockwise from north) and is inclined by either 26 or 154° (±1°) from the sky plane. While the Doppler shifts seen in carbon monoxide show that the north side of the disk is rotating towards us (Fig. 2), thus constraining the ascending node to be north of the star, the inclination remains ambiguous because the disk could be rotating either clockwise or anti-clockwise as projected on the sky. That is, these observations do not distinguish whether the east or west side of the disk is closer to Earth.

Of the two possible disk orientations, the 154° case is only 4° away from the polar configuration (that is, it is perpendicular to both the BaBb orbital plane and the BaBb pericentre direction), while the 26° case is inclined 48° from the BaBb binary plane (which we refer to as the 'moderately' misaligned case). The uncertainty on these relative angles is about 4°, so the polar orientation is consistent with being perfectly polar. Given the small chance that a randomly chosen orientation should appear to be in the polar configuration, which is expected based on the dynamics and models discussed above, this configuration is by far the most likely interpretation. That is, the theoretical models provide a prior that leads us to favour the polar configuration, and a sketch is shown in Fig. 3.

To further test this hypothesis, we simulated the response of the disk to perturbations from the stellar orbits using both gas-free '*n*-body' and fluid-based smoothed particle hydrodynamics (SPH) simulations (see Methods). The main conclusion from the *n*-body simulations is that test particles placed on circular orbits at the observed 2.5–4.6 AU radial location of the dust are generally ejected within fewer than 1 Myr, regardless of the disk orientation.

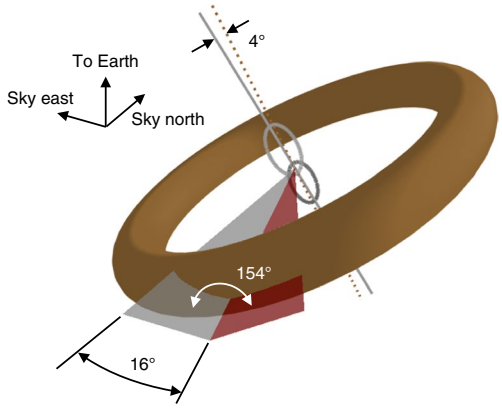

Fig. 3 | Three-dimensional sketch of the polar configuration. Grey ellipses show the orbit of the BaBb binary, and the torus shows the surrounding disk. The axes are indicated by the three labelled arrows. The two triangular planes show the plane of the sky (grey) and disk (red), which intersect at an angle of 16° from south (that is, the disk position angle). The angle between these planes is the disk inclination of 154°. Grey lines show the angular momentum vector of the disk **Lc** (dotted), and the binary pericentre direction **ωb** (solid), both of which point away from Earth. These vectors are aligned within 4°, meaning that for this orientation, the disk plane is almost perfectly perpendicular to both the binary orbital plane and the pericentre direction.

Independent of the disk orientation, we therefore conclude that the dust observed with ALMA is embedded within a more massive gas disk, which acts to stabilize the disk against both interior and exterior stellar perturbations. Our estimates of the gas and dust mass in the disk are consistent with this picture, but do not confirm it because they have large systematic uncertainties (see Methods). The *n*-body dynamics, in concert with the detection of carbon monoxide, oxygen and hydrogen gas, therefore suggest that HD 988000BaBb almost certainly harbours a long-lived gas-rich protoplanetary disk.

Our fluid-based simulations find that torques from the inner binary reorient a gas disk in the moderately misaligned configuration to the polar configuration in several hundred years. In contrast, the polar configuration is stable and remains in the observed state for at least 500 BaBb orbits (430 years). While the timescale for this evolution depends on the specific assumptions made for the simulations (for example, the disk scale height and viscosity) and may be longer than found by our simulations, theory suggests that disks will typically become aligned within a few million years[5,10]. The reorientation time is therefore expected to be shorter than the system age of about 10 Myr, and we conclude that the most probable interpretation is that the disk is in the polar configuration.

While we cannot currently detect planets within the HD 98800 disk (the high optical depth and small angular scale hamper imaging, and radial velocity precision is limited for young binaries), our data do show evidence of dust growth. Specifically, our models find that the gas is more radially extended than the bulk of the dust (see also Fig. 2). While the derived edge locations reflect the sensitivity of the observations to some degree, these models account for all of the carbon monoxide surface brightness, and for 99% of the dust. The dust surface brightness is a factor of 100 lower at 5.5 au compared with 3.5 au, which is much larger than the factor of 2 expected if the dust emission scaled with the brightness of the gas emission over this distance. Similar differences in gas and dust radial extent are seen for disks around single stars, and are thought to be caused by inward radial drift of dust particles that have grown beyond micrometres in size and/or the in situ growth of dust to sizes large enough that their mm-wave emission is fainter at larger distances[26,27]. Our models therefore show probable evidence of the effects of grain growth on radial disk structure, and therefore the same evidence of the first steps towards planet formation seen in equivalent disks around single stars.

How did this system form? Simulations suggest that such outcomes may be a natural result of the chaotic nature of star formation[2]. One possibility is that two initially separate binary systems became gravitationally bound, and misaligned HD 98800BaBb's disk in the process (and perhaps destroyed any disk around A). However, simulations show that formation from molecular cloud material with a range of angular momenta can result in misaligned disks in isolated systems[2], and indeed such systems are observed[7], so it does not appear that the presence of an exterior companion is a necessary condition for forming misaligned circumbinary disks. The IRS 43 system, with a circumbinary disk misaligned by about 60°, is a possible example of what systems such as HD 98800 could look like earlier in their evolution before binary torques reorient the disk (albeit on a scale of tens of au, rather than a few au)[7].

We may also ask whether polar circumbinary disks might be common. Assuming disks that are initially randomly orientated relative to the binary orbital plane and that are not massive enough to affect the binary orbit, and that binary eccentricities are uniformly distributed up to $e=0.8$ (ref. [28]), the fraction of disks that should evolve to a polar configuration is 46% (see Supplementary Information). If planet formation can proceed equally efficiently in both coplanar and polar configurations, circumbinary planets on polar orbits are predicted to be nearly as common as their coplanar brethren (although these fractions may be modified by later dynamical evolution[29]). The most eccentric binaries are the most likely to have polar disk configurations, so it is not surprising that the known transiting circumbinary planets, which are near to coplanar, are all in systems with $e \leq 0.52$, with 8 out of 9 having $e < 0.22$ (refs. [30,31]). Polar disks, and perhaps planets, may be a common outcome of circumbinary disk formation, and provide motivation for systematic searches for both.

Methods

Observations and data processing. HD 98800 was observed by ALMA in band 6 (1.3 mm) in two observing blocks on 2017 November 15 and 19; 49 antennas were used in the first block and 45 in the second. The shortest and longest baselines were 92 m and 11.8 km. The correlator configuration used 3 broad continuum windows with 2 GHz bandwidth, and 1 centred on the carbon monoxide $J=2$–1 line with a spectral resolution of 488 kHz (0.73 km s^{-1} velocity resolution). Each block comprised observations of HD 98800, interspersed with observations of phase calibrator J1104-2431. J1127-1857 was used as the bandpass and flux calibrator. The time on-source was 34 min for each block. The raw data were calibrated using the observatory pipeline with CASA version 5.1.

The data were further processed using one cycle of phase self-calibration to improve the signal-to-noise ratio. All spectral windows were combined, and the averaging time ('solint') was chosen to be relatively long (20–40 min) to avoid flagging antennas due to low signal-to-noise ratio, thereby retaining maximal spatial resolution. The root mean square (RMS) variations measured in clean images before self-calibration with Briggs weighting (robust = 0.5) were 27 and 32 μJy beam^{-1} for the first and second observations. After self-calibration, these were 20 and 18 μJy beam^{-1}. Attempts at further self-calibration did not improve the signal-to-noise ratio.

Following calibration, the two observations were concatenated into a single set of visibilities for imaging and modelling. This combination was verified to be reasonable by modelling the continuum of each observation separately (as described below), which found that the sky offsets of the disk were consistent to within 0.0002 arcsec (0.01 au). The difference in integrated flux densities was consistent to within 1%. In the final Briggs-weighted clean image, the beam size is 46 × 42 mas, the RMS is 14 μJy beam^{-1} and the peak signal-to-noise ratio is 280. In a naturally weighted image, the beam size is 64 × 56 mas, the RMS is 13 μJy beam^{-1} and the peak signal-to-noise ratio is 450. In a uniformly weighted image, the beam size is 32 × 25 mas^2, the RMS is 43 μJy beam^{-1} and the peak signal-to-noise ratio is 46.

For continuum modelling, a single spectral window from the combined observations was used (the first, centred at 1.311 mm) with the 2 GHz bandwidth averaged into 4 channels. While more data could have been used, the continuum signal-to-noise ratio is easily sufficient to obtain stringent modelling constraints with one spectral window. Visibility data were time-averaged into 20 s chunks,

then exported to a text file and modelled as outlined below. The weights associated with each visibility were divided by a re-weighting factor such that a null model produces a χ^2 value of 1, based on the expectation that each individual visibility measurement has negligible signal-to-noise ratio[32]. The re-weighting factor was 5.8 (which is decreased to 2.6 if the CASA `statwt` task is run first).

For gas modelling, the window centred on the carbon monoxide $J=2$–1 line was used. The continuum was subtracted using the CASA `uvcontsub` task, the two observations merged using the `mstransform` task and 40 channels near the carbon monoxide line extracted to a series of text files containing the visibilities at each frequency (or equivalently, velocity). A re-weighting factor was again used, which was within a few percent of 1. A naturally weighted clean carbon monoxide cube has a beam size of 61×54 mas^2, an RMS of 0.8 mJy beam^{-1} in each 0.73 km s^{-1} channel and a typical peak signal-to-noise ratio of 4–6 depending on the channel. The intensity-weighted carbon monoxide velocity (moment 1) map is shown in Fig. 2, and the velocity-integrated carbon monoxide (moment 0) map is shown in Supplementary Fig. 1. Channel maps are shown in the upper panel of Supplementary Fig. 3, where the data have been further averaged to show only 20 channels.

HD 98800 has been observed at millimetre wavelengths many times in the past with single-dish telescopes. These show a considerable degree of scatter, with ref. [33] measuring 30.7 ± 8.2 and 54.4 ± 3.61 mJy at 1.3 mm with the Caltech Submillimeter Observatory (CSO) and Institut de Radioastronomie Millimétrique (IRAM) 30-m telescope, respectively. Our modelling below yields a total disk flux of 47.4 ± 0.4 mJy. Including an absolute calibration uncertainty of 10% yields a final flux measurement of 47 ± 5 mJy. Our value is not significantly below the previous single-dish measurements, so it is unlikely that we have resolved out significant flux. We discuss the dust mass briefly in the Supplementary Information.

The phase centre of the observations is not perfectly centred on either AaAb, BaBb or the system photocentre, no doubt caused by some uncertainty in the actual position of the system components and their relative motions, as derived by Hipparcos[14]. As another output of the modelling, assuming that the BaBb barycentre is at the centre of the disk, at the time of the observation (2017.874), we find that BaBb is centred at $\alpha=11$ h 22 min 05.17437 s, $\delta=-24$ deg 46 min 39.5043 s (170.52155986°, −24.77764009°). The positional uncertainty from the modelling is ±0.0001 arcsec, but the true uncertainty is limited by ALMA's pointing accuracy, which the Technical Handbook suggests is about 0.03 arcsec.

Visibility modelling. Modelling of the continuum and carbon monoxide data was done in the visibility plane using an optically thin line-of-sight integration code. While the dust is probably optically thick, the use of a radiative transfer code would make little difference here because the disk is close to face on, and we are therefore simply modelling the surface brightness of the disk as a function of the radius. A function specifies the three-dimensional disk density in spherical polar coordinates, which is mapped into a three-dimensional Cartesian volume using two or three rotations (the position angle Ω, the inclination i and the argument of pericentre ω where necessary). Two axes of this cube represent the sky plane and the third the line of sight, and the final continuum image of a given model is created by summing the cube along the line of sight axis. Velocity cubes are created by first computing the radial velocity at each location in the cube. Layers in the velocity cube are again the sum along the line-of-sight axis, but only including pixels from the cube that are within the velocity range for a given layer.

The range of models that are consistent with the data are found using the Markov chain Monte Carlo package `emcee`[34]. The log-likelihood $-\chi^2/2$ of each model is computed given the visibility data using GALARIO[35]. GALARIO also computes the pixel size and image extent necessary for sufficient resolution in the Fourier-plane baseline distances u and v when the images are transformed into visibilities, which are 4.6 milliarcsec per pixel and 2,048 pixels.

The strongest signal in the continuum image in Fig. 1 is a narrow ring of dust emission, so we model this ring to derive constraints on the structure and reveal any lower-level emission. For both continuum and carbon monoxide, we use a simple power-law density model, where the dust or gas lies between two limiting radii, r_{in} and r_{out}, and where the volume density is a power-law function of the radius r^{α}. The density is specified in a given pixel in the cube, and the vertical scale height is a fixed fraction of the radial distance, so the surface density is $\propto r^{\alpha+1}$. The vertical density structure is Gaussian with the scale height fixed to $0.05r$ for all models, as for a nearly face-on disk this parameter is poorly constrained. For the continuum model, we found that the fit was significantly improved if the disk inner edge has a small eccentricity e_{in}, which was implemented by varying r_{in} as a function of the azimuth. Further parameters are the sky offsets x_0 and y_0, the disk position angle east of north Ω and the inclination i, and the argument of pericentre ω. The images are scaled by the total flux F (in the two-dimensional image for continuum, or the three-dimensional cube for carbon monoxide). There are therefore eight parameters for the continuum model (x_0, y_0, Ω, ω, i, F, r_{in}, r_{out}, α and e_{in}). The density is multiplied by an emission function that mimics the Rayleigh–Jeans tail of a blackbody (that is, $\propto 1/\sqrt{r}$). The radial dependence of this function is largely arbitrary as it is degenerate with α, and while it is a reasonable approximation for the dust seen in the continuum, the temperature dependence for carbon monoxide may be different. For the carbon monoxide model, the eccentric inner-edge parameters ω and e_{in} are not necessary as the signal-to-noise ratio is much lower, but an additional parameter—the systemic velocity of HD 98800 BaBb, v_{sys}—is needed. We assume that the carbon monoxide orbits a single point mass with a combined mass of HD 98800BaBb of $1.28M_{\odot}$[17].

While it is likely that the carbon monoxide and dust are optically thick, we found that our models were sufficient to reproduce the data. We tried modelling the data with a simple optical depth prescription where the observed surface brightness in the model sky images was attenuated by a further free parameter τ_{SB} via $1-e^{-SB/\tau_{SB}}$ (that, is τ_{SB} is the surface brightness at which the emission becomes optically thick), but we found that these models were consistent with $\tau_{SB}=0$ (and the other parameters unchanged), and therefore that this additional complication is not necessary to obtain constraints on the disk extent and spatial orientation.

Continuum modelling results. The best-fitting continuum model was found using 64 'walkers' (parallel Markov chain Monte Carlo chains) run for 1,000 steps (having discarded a prior 'burn-in' run of 1,000 steps). The best-fit parameters derived from the posterior distributions are given in Supplementary Table 1. The y offset y_0 is relatively large because the observation phase centre is offset from BaBb, as described above. The main parameters of interest here are the disk orientation Ω and i, and the dust extent from r_{in} to r_{out}, which are discussed in the main text.

Initial attempts to model the continuum with axisymmetrical models left asymmetrical residuals suggestive of an offset near the inner disk edge, which motivated the use of an eccentric inner disk edge. While this parameterization may not be representative of the true structure, our finding that the best-fit e_{in} is significantly greater than zero shows that the disk is not axisymmetrical, and that this asymmetry lies near the inner disk edge. The position angle of the pericentre is given by the parameter ω; as it is measured from the ascending node, the best-fit value of −73° means that the disk is closest to the binary towards the north-west (that is, a position angle of approximately $-72+16=-56$°). While it is tempting to make comparisons with the simulations in Supplementary Fig. 6, these show gas density and the observed asymmetry is in the dust. Nevertheless, it is likely that the preference for a non-zero inner edge eccentricity results from perturbations from the inner binary, and the structure may be characterized in more detail with higher-resolution continuum imaging, and deeper- and/or lower-spatial-resolution line imaging.

Residual images are shown in Supplementary Fig. 2, which shows that our model reproduces nearly all of the observed continuum structure. The peak signal-to-noise ratio in the original naturally weighted continuum image for the same spectral window is 300, meaning that the residuals are at most only 1% of the peak. Some emission remains beyond the bright ring at 2–4σ, suggestive of low-level dust emission that might be recovered more strongly in lower-resolution images. Some residual emission is also seen interior to the ring, which might arise from dust entrained in gas that is flowing towards and accreting onto the inner binary, and be related to our finding that the inner disk edge is asymmetrical. Accreting material may provide an explanation for the facts that HD 98800 was reported to be photometrically variable by Hipparcos[36] and that HD 98800B suffers significantly more dust extinction than A[17,19,36,37].

Carbon monoxide modelling results. Channel maps near the systemic velocity of HD 98800BaBb are shown in the upper panel of Supplementary Fig. 3. The best-fitting carbon monoxide velocity model was found using 64 walkers run for 1,000 steps, where 1,000 prior steps were discarded as a burn-in. The best-fit parameters derived from the posterior distributions are given in Supplementary Table 2. The residuals after subtraction of the best-fitting model are shown in the lower panel of Supplementary Fig. 3. The carbon monoxide disk orientation is consistent with the continuum model results shown in Supplementary Table 2, but the carbon monoxide disk covers a greater radial extent—from 1.6–6.4 AU, compared with 2.5–4.6 AU.

The peak level of channel emission in Supplementary Fig. 3 is approximately 5 mJy beam^{-1}, which we find is consistent with that expected from optically thick carbon monoxide at an excitation temperature of 70 K. A lower excitation temperature would yield a lower flux than observed, while a higher excitation temperature would yield a higher flux, or could originate from optically thin carbon monoxide. We discuss the carbon monoxide mass and gas-to-dust ratio briefly in the Supplementary Information.

Simulations. *n*-body. We simulated the system as gas free using the REBOUND code[38], to test where particles could orbit in the absence of stabilizing forces that would arise if the gas mass is comparable to or greater than the dust mass (see also ref. [39]). We modelled the inner binary BaBb using the best-fit parameters from ref. [17], the outer binary AaAb as a single object, the AB orbit as derived in the Supplementary Information, and all other particles as massless. The disk appears largely circular based on the continuum modelling, so we initialized particles on circular orbits in one of the two possible disk orientations at a range of true anomalies, and ran simulations for 1 Myr. We used the 'whfast' integrator[40] with a time step of one-twentieth of the BaBb orbital period. Particles with distances more than 2,000 AU from the system centre of mass are removed and their removal time recorded; while the integration method does not allow collisions or compute close encounters accurately, these events soon lead to particle ejection anyway.

The results are shown in Supplementary Fig. 5 and show that in the gas-free case test, particles do not survive for 1 Myr in the moderately inclined disk configuration. Particles in the polar configuration do survive for up to 1 Myr, but only at semi-major axes between 5 and 7 au and a very narrow band near 4 au, and neither region is consistent with the extent seen in the continuum with ALMA. In both configurations, particles beyond 7 au are typically removed in 5,000 years; comparing this time with the 250-year period of the AB binary suggests that short-term interactions are the cause (that is, the removal time is tens of AB orbits, not hundreds or thousands, which would suggest long-term secular effects), and therefore that 7 au is the approximate outer disk truncation radius imposed by A.

These results therefore indicate that gas-free dynamics do not apply to the dust observed between 2.5 and 4.6 au around HD 98800BaBb, and that the dust is almost certainly strongly influenced and stabilized by gas. The disk is therefore probably gas rich (that is, the gas mass is greater than the dust mass) and, given the detection of hydrogen gas emission[25], probably still in the primordial protoplanetary disk phase.

SPH. We used `Phantom`[41] to simulate the response of the two possible disk configurations to perturbations from the inner binary, assuming a gas-rich protoplanetary disk. The simulations were run for 500 orbits of the inner binary (430 years). We did not include the outer binary, as the disk was found to change orientation on a shorter timescale (~100 years) than the period of the outer binary (~250 years). This timescale difference of course does not mean that A has no effect on the disk around B, since test particles in the polar configuration are truncated at around 7 au, which is near the outer extent of the detected carbon monoxide.

For the disk, the simulations used the same SPH parameters as ref. [4] and 300,000 particles. While we cannot be sure that these specific parameters apply to HD 98800's disk, theory suggests that real disks are likely to become aligned before they disperse[5,9,10]. While the absolute timescales derived from our simulations may be inaccurate, as the disk scale height and viscosity could be different, the evolution is likely to be similar.

The results of simulations of the two configurations are shown in Supplementary Fig. 6, where the left set of panels shows the moderately misaligned case and the right panels the polar case (the images were created using `splash`[42]). In each pair of images, the left subpanels show the disk density projected onto the sky plane, and the right panel a side view. The time evolution (moving down the panels) shows that the polar configuration does not significantly change orientation, while the moderately misaligned case does. In fact, the moderately misaligned disk eventually reaches the polar configuration, although it has been significantly perturbed and disrupted in the process. Thus, we conclude that the polar disk configuration is by far the best interpretation of the data, as the lifetime of the disk in the moderately misaligned case is very short relative to the stellar age of ten million years. Because the time taken to reorient the disk is short relative to the AB orbital period, and the effect of A where the disk is observed is minimal, including A in the simulations would not change this conclusion.

Some spiral structure has been induced in the disk in the polar case; if the HD 98800 disk has similar structure, these perturbations may be the cause of the asymmetry that requires the continuum model to have non-zero e_{in}.

Data availability

The ALMA data used in this study are available in the ALMA Science Archive (project code 2017.1.00350.S). Post-processing, modelling and other code used in this study are available on GitHub at https://github.com/drgmk/hd98800_alma_c5. Post-processed data that support the plots within this paper and other findings of this study are available from the corresponding author upon reasonable request.

Received: 17 August 2018; Accepted: 28 November 2018;
Published online: 14 January 2019

References

1. Zhu, W., Petrovich, C., Wu, Y., Dong, S. & Xie, J. About 30% of Sun-like stars have Kepler-like planetary systems: a study of their intrinsic architecture. *Astrophys. J.* **860**, 101 (2018).
2. Bate, M. R. On the diversity and statistical properties of protostellar discs. *Mon. Not. R. Astron. Soc.* **475**, 5618–5658 (2018).
3. Aly, H., Dehnen, W., Nixon, C. & King, A. Misaligned gas discs around eccentric black hole binaries and implications for the final-parsec problem. *Mon. Not. R. Astron. Soc.* **449**, 65–76 (2015).
4. Martin, R. G. & Lubow, S. H. Polar alignment of a protoplanetary disk around an eccentric binary. *Astrophys. J. Lett.* **835**, L28 (2017).
5. Zanazzi, J. J. & Lai, D. Inclination evolution of protoplanetary discs around eccentric binaries. *Mon. Not. R. Astron. Soc.* **473**, 603–615 (2018).
6. Rodriguez, D. R., Kastner, J. H., Wilner, D. & Qi, C. Imaging the molecular disk orbiting the twin young suns of V4046 Sgr. *Astrophys. J.* **720**, 1684–1690 (2010).
7. Brinch, C., Jørgensen, J. K., Hogerheijde, M. R., Nelson, R. P. & Gressel, O. Misaligned disks in the binary protostar IRS 43. *Astrophys. J. Lett.* **830**, L16 (2016).
8. Farago, F. & Laskar, J. High-inclination orbits in the secular quadrupolar three-body problem. *Mon. Not. R. Astron. Soc.* **401**, 1189–1198 (2010).
9. Foucart, F. & Lai, D. Assembly of protoplanetary disks and inclinations of circumbinary planets. *Astrophys. J.* **764**, 106 (2013).
10. Lubow, S. H. & Martin, R. G. Linear analysis of the evolution of nearly polar low-mass circumbinary discs.*Mon. Not. R. Astron. Soc.* **473**, 3733–3746 (2018).
11. Martin, R. G. & Lubow, S. H. Polar alignment of a protoplanetary disc around an eccentric binary—II. Effect of binary and disc parameters. *Mon. Not. R. Astron. Soc.* **479**, 1297–1308 (2018).
12. Haisch, K. E. Jr., Lada, E. A. & Lada, C. J. Disk frequencies and lifetimes in young clusters. *Astrophys. J. Lett.* **553**, L153–L156 (2001).
13. Kennedy, G. M. et al. 99 Herculis: host to a circumbinary polar-ring debris disc. *Mon. Not. R. Astron. Soc* **421**, 2264–2276 (2012).
14. Van Leeuwen, F. Validation of the new Hipparcos reduction. *Astron. Astrophys.* **474**, 653–664 (2007).
15. Kastner, J. H., Zuckerman, B., Weintraub, D. A. & Forveille, T. X-ray and molecular emission from the nearest region of recent star formation. *Science* **277**, 67–71 (1997).
16. Barrado Y Navascués, D. On the age of the TW Hydrae association and 2M1207334-393254. *Astron. Astrophys.* **459**, 511–518 (2006).
17. Boden, A. F. et al. Dynamical masses for low-mass pre-main-sequence stars: a preliminary physical orbit for HD 98800 B. *Astrophys. J.* **635**, 442–451 (2005).
18. Walker, H. J. & Wolstencroft, R. D. Cool circumstellar matter around nearby main-sequence stars. *Publ. Astron. Soc. Pac.* **100**, 1509–1521 (1988).
19. Akeson, R. L. et al. The circumbinary disk of HD 98800B: evidence for disk warping. *Astrophys. J.* **670**, 1240–1246 (2007).
20. Andrews, S. M. et al. Truncated disks in TW Hya association multiple star systems. *Astrophys. J.* **710**, 462–469 (2010).
21. Ribas, Á., Macías, E., Espaillat, C. C. & Duchêne, G. Long-lived protoplanetary disks in multiple systems: the VLA view of HD 98800. *Astrophys. J.* **865**, 77 (2018)..
22. Furlan, E. et al. HD 98800: a 10 Myr old transition disk. *Astrophys. J.* **664**, 1176–1184 (2007).
23. Wyatt, M. C. et al. Transience of hot dust around Sun-like stars. *Astrophys. J.* **658**, 569–583 (2007).
24. Riviere-Marichalar, P. et al. Gas and dust in the TW Hydrae association as seen by the Herschel Space Observatory. *Astron. Astrophys.* **555**, A67 (2013).
25. Yang, H. et al. A far-ultraviolet atlas of low-resolution Hubble Space Telescope spectra of T Tauri stars. *Astrophys. J.* **744**, 121 (2012).
26. Andrews, S. M. et al. The TW Hya disk at 870 μm: comparison of CO and dust radial structures. *Astrophys. J.* **744**, 162 (2012).
27. Facchini, S., Birnstiel, T., Bruderer, S. & van Dishoeck, E. F. Different dust and gas radial extents in protoplanetary disks: consistent models of grain growth and CO emission. *Astron. Astrophys.* **605**, A16 (2017).
28. Raghavan, D. et al. A survey of stellar families: multiplicity of solar-type stars. *Astrophys. J. Suppl. Ser.* **190**, 1–42 (2010).
29. Muñoz, D. J. & Lai, D. Survival of planets around shrinking stellar binaries.*Proc. Natl Acad. Sci. USA* **112**, 9264–9269 (2015).
30. Martin, D. V., Mazeh, T. & Fabrycky, D. C. No circumbinary planets transiting the tightest Kepler binaries—apossible fingerprint of a third star. *Mon. Not. R. Astron. Soc.* **453**, 3554–3567 (2015).
31. Kostov, V. B. et al. Kepler-1647b: the largest and longest-period Kepler transiting circumbinary planet. *Astrophys. J.* **827**, 86 (2016).
32. Guilloteau, S., Dutrey, A., Piétu, V. & Boehler, Y. A dual-frequency sub-arcsecond study of proto-planetary disks at mm wavelengths: first evidence for radial variations of the dust properties. *Astron. Astrophys.* **529**, A105 (2011).
33. Walker, H. J. & Butner, H. M. Follow-up observations of β-pic-like stars. *Astrophys. Space Sci.* **224**, 389–393 (1995).
34. Foreman-Mackey, D., Hogg, D. W., Lang, D. & Goodman, J. emcee: the MCMC hammer. *Publ. Astron. Soc. Pac.* **125**, 306–312 (2013).
35. Tazzari, M., Beaujean, F. & Testi, L. GALARIO: a GPU accelerated library for analysing radio interferometerobservations. *Mon. Not. R. Astron. Soc.* **476**, 4527–4542 (2018).
36. Soderblom, D. R. et al. HD 98800: a unique stellar system of Post-T Tauri stars. *Astrophys. J.* **498**, 385–393 (1998).
37. Tokovinin, A. A. The visual orbit of HD 98800. *Astron. Lett.* **25**, 669–671 (1999).
38. Rein, H. & Liu, S.-F. REBOUND: an open-source multi-purpose N-body code for collisional dynamics. *Astron. Astrophys.* **537**, A128 (2012).
39. Doolin, S. & Blundell, K. M. The dynamics and stability of circumbinary orbits.*Mon. Not. R. Astron. Soc.* **418**, 2656–2668 (2011).
40. Rein, H. & Tamayo, D. WHFAST: a fast and unbiased implementation of a symplectic Wisdom–Holman integrator for long-term gravitational simulations. *Mon. Not. R. Astron. Soc.* **452**, 376–388 (2015).

41. Price, D. J. et al. Phantom: a smoothed particle hydrodynamics and magnetohydrodynamics code for astrophysics. *Publ. Astron. Soc. Aust.* **35**, e031 (2018).
42. Price, D. J. splash: an interactive visualisation tool for smoothed particle hydrodynamics simulations. *Publ. Astron. Soc. Aust.* **24**, 159–173 (2007).

Acknowledgements

G.M.K. is supported by the Royal Society as a Royal Society University Research Fellow. L.M. acknowledges support from the Smithsonian Institution as a Submillimeter Array Fellow. O.P. is supported by the Royal Society Dorothy Hodgkin Fellowship. S.F. acknowledges an ESO Fellowship. We thank A. Ribas for sharing the Very Large Array image of HD 98800. This paper makes use of the following ALMA data: ADS/JAO.ALMA#2017.1.00350.S. ALMA is a partnership of the ESO (representing its member states), NSF (United States) and NINS (Japan), together with NRC (Canada), MOST and ASIAA (Taiwan), and KASI (Republic of Korea), in cooperation with the Republic of Chile. The Joint ALMA Observatory is operated by ESO, AUI/NRAO and NAOJ.

Author contributions

G.M.K. conceived the project, analysed the data, carried out the modelling and wrote the manuscript. L.M. contributed gas calculations and provided advice on self-calibration. B.M.Y. set up and ran the *n*-body simulations. D.P. provided advice on running the smoothed particle hydrodynamics simulations. All co-authors provided input on the manuscript.

Competing interests

The authors declare no competing interests.

Additional information

Supplementary information is available for this paper at https://doi.org/10.1038/s41550-018-0667-x.

Reprints and permissions information is available at www.nature.com/reprints.

Correspondence and requests for materials should be addressed to G.M.K.

Publisher's note: Springer Nature remains neutral with regard to jurisdictional claims in published maps and institutional affiliations.